Water Oxidation

Nanostructured Cobalt Oxide Clusters in Mesoporous Silica as Efficient Oxygen-Evolving Catalysts**

Feng Jiao and Heinz Frei

The development of integrated artificial photosynthetic systems for the direct conversion of carbon dioxide and water to fuel depends on the availability of efficient and robust catalysts for the chemical transformations. Catalysts need to exhibit turnover frequency (TOF) and density (hence size) commensurate with the solar flux at ground level ($1000\ W\,m^{-2}$, airmass (AM) 1.5)[1] to avoid wasting of incident solar photons. For example, a catalyst with a TOF of $100\ s^{-1}$ requires a density of one catalytic site per square nanometer. Catalysts with lower rates or taking up a larger space will require a high-surface-area, nanostructured support that affords tens to hundreds of catalytic sites per square nanometer. Furthermore, catalysts need to operate close to the thermodynamic potential of the redox reaction so that a maximum fraction of the solar photon energy is converted to chemical energy. Stability considerations favor all-inorganic oxide materials, as does avoidance of harsh reaction conditions of pH value or temperature.

For the water oxidation half reaction, iridium oxide is a material that essentially fulfils these requirements. After early reports that identified IrO_2 particles as robust water oxidation catalysts,[2–4] Mallouk and co-workers determined a TOF for Ir oxide colloidal particles of $40\ s^{-1}$ in aqueous solution (pH 5.7, 25°C).[5–7] In this work, the catalyst was driven by a $[Ru^{3+}(bpy)_3]$ unit (bpy = 2,2′-bipyridine) generated photochemically with visible light using the established $[Ru^{2+}(bpy)_3]$/persulfate system with a modest overpotential (η) of 370 mV. For IrO_2 colloidal particles coated on an indium tin oxide anode, Yagi et al. obtained TOF = $7\ s^{-1}$ (pH 5.3, 25°C, $\eta = 570$ mV) from electrochemical measurements.[8] We have recently demonstrated that all-inorganic photocatalytic units consisting of IrO_2 nanoclusters (ca. 2 nm) directly coupled to a single-center chromium(VI) or a binuclear $TiCr^{III}$ charge-transfer chromophore afford oxygen evolution under visible light with good quantum yield.[9,10] While iridium oxide closely approaches the efficiency and stability required for a water oxidation catalyst in a solar conversion system, iridium is the least abundant metal on earth and is not suitable for use on a very large scale. Therefore, it is imperative to explore oxides of the much more abundant first-row transition metals, as inspired by nature's Mn_4Ca cluster of photosystem II.[11] Herein, we focus on Co_3O_4 nanoclusters as candidates for water oxidation catalysts under mild conditions.

Numerous electrochemical studies of cobalt and manganese oxides as catalytic materials for oxygen evolution have been conducted over the past decades. For the purpose of evaluating metal oxides in the form of nanometer-sized clusters as catalytic components for water oxidation, comparisons of turnover frequencies are most relevant. Such values were typically not reported in electrochemical studies, but lower limits can be calculated in cases where the amount of catalyst material was indicated. The data are summarized in Table S1 of the Supporting Information ("lower limits" refers to the assumption that all deposited metal centers are catalytically active).[12] Briefly, for Co_3O_4 (spinel), lower limits of TOF ranging from 0.020 to $0.0008\ s^{-1}$ at high pH values and temperatures between 25 and 120°C were derived from work by Schmidt, Iwakura, Rasiyah, and Singh et al.[13–16] Using an in situ activation method for developing a cobalt-based electrocatalytic film,[13] Kanan and Nocera reported very recently oxygen evolution from pH-neutral, phosphate-buffered aqueous solution for which a TOF ≥ $0.0007\ s^{-1}$ ($\eta = 410$ mV) is estimated.[12,17] A study at neutral pH values and room temperature using an anode coated with MnO_2 by Morita et al. gave TOF ≥ $0.013\ s^{-1}$ ($\eta = 440$ mV).[18] Using silicon-doped nanostructured Fe_2O_3 topped by a Co monolayer as photocatalytic anode material, Grätzel reported high incident photon-to-current efficiency at negligible overpotential in photoelectrochemical water oxidation.[19] Furthermore, oxygen evolution was reported by Harriman et al. from aqueous suspensions of micrometer-sized Co_3O_4 or Mn_2O_3 particles using the photochemical $[Ru^{2+}(bpy)_3]$/persulfate method (pH 5, room temperature, $\eta = 325$ mV).[4] Data presented in that study indicate TOF between 0.035 and $0.055\ s^{-1}$. The photochemical and electrochemical results of studies with cobalt and manganese oxides clearly suggest that these materials hold promise for developing robust, efficient, nanometer-sized catalysts for water oxidation.

[*] Dr. F. Jiao, Dr. H. Frei
Physical Biosciences Division
Lawrence Berkeley National Laboratory
University of California, Berkeley, CA 94720 (USA)
Fax: (+1) 510-486-7768
E-mail: HMFrei@lbl.gov

Communications

Herein we report efficient oxygen evolution at nanostructured Co_3O_4 clusters in mesoporous silica in aqueous solution under mild temperature and pH conditions for the first time. The catalyst was driven by the $[Ru^{2+}(bpy)_3]$/persulfate sensitizer system under visible light.

Typical TEM images of Co_3O_4 nanoclusters prepared in SBA-15 silica at 4.2 and 8.6 wt% loading (as determined by inductively coupled plasma mass spectrometer (ICP-MS)) by wet impregnation are shown in Figure 1 a,b.[12,20–22] The images show that the integrity of the silica channel structure
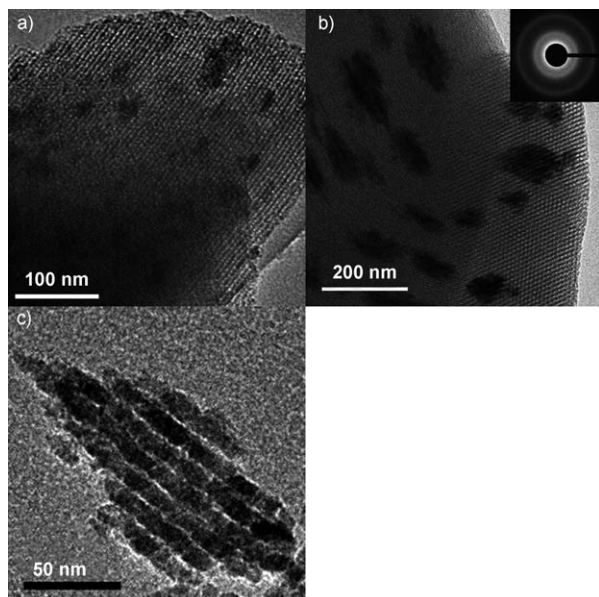

Figure 1. TEM images of a) SBA-15/Co_3O_4 4% loading, b) SBA-15/Co_3O_4 8% loading, c) Co_3O_4 nanocluster (8% sample) after removal of the SBA-15 silica material using aqueous NaOH as etching reagent. The inset in (b) shows the SAED pattern.

(diameter 8 nm) was maintained upon formation of the Co_3O_4 clusters. By examining many SBA-15 particles in different regions of the powder, we confirmed that Co_3O_4 nanoclusters are formed exclusively inside the mesopores. The spheroid-shaped clusters consist of parallel bundles of nanorods whose structure is imposed by the silica channels. The rods are linked by short bridges, formed by Co_3O_4 growth in the micropores interconnecting the mesoscale channels.[22] TEM images of the Co_3O_4 clusters were recorded after removal of the silica scaffold by heating of a suspension of the SBA-15/Co_3O_4 sample in aqueous NaOH (2 M) at 60 °C for 30 min. As an example, Figure 1 c shows a cluster isolated from the 8% sample. Analysis of numerous clusters shows that for the 4% sample, the average Co_3O_4 spheroid-shaped bundle has a short diameter of 35 nm and a long diameter of 65 nm (histogram analysis shown in Figure S2 in the Supporting Information).[12] For the 8% sample, the average bundle of nanorods makes a spheroid with short and long diameters of 65 and 170 nm, respectively.

Selected area electron diffraction (SAED) images (Figure 1 b, inset) confirm the crystalline nature of the large Co_3O_4 nanoclusters (8% sample). By contrast, no clear

diffraction pattern was observed for the 4% sample, suggesting that the 35 nm clusters are poorly crystallized. These findings are confirmed by powder X-ray diffraction (XRD) measurements (Figure 2). The diffraction peaks of the bulk Co_3O_4 phase (trace a) are characteristic for Co_3O_4 (spinel
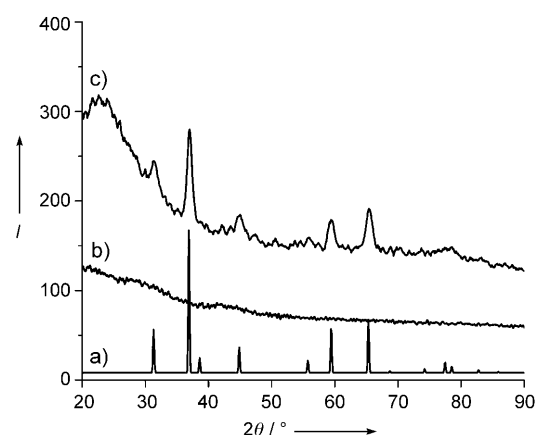

Figure 2. Wide-angle powder XRD patterns for a) micrometer-sized Co_3O_4 particles, b) SBA-15/Co_3O_4 (4%), c) SBA-15/Co_3O_4 (8%).

structure). The same peaks are clearly visible in the pattern of the Co_3O_4 clusters of the 8% sample (trace c) but are absent in the 4% sample (trace b). The absence of diffraction peaks for the 35 nm clusters indicates that the crystalline domains are very small (at most a few nanometers) and points to polycrystallinity. The width of the XRD bands in the case of the 8% sample corresponds to a 7.6 nm object according to the Scherrer formula, in agreement with the expected diameter of Co_3O_4 nanorods imposed by the SBA-15 channel structure (Figure 1). Fourier transformed extended X-ray absorption fine structure (EXAFS) data for micrometer-sized Co_3O_4 particles and Co_3O_4 nanoclusters of 8% and 4% loaded SBA-15 are shown in Figure 3. The perfect agreement between the spectra of bulk Co_3O_4 (——) and SBA-15/Co_3O_4(8%) (– – –) confirms the well-crystallized spinel structure of the large clusters, consistent with the SAED and
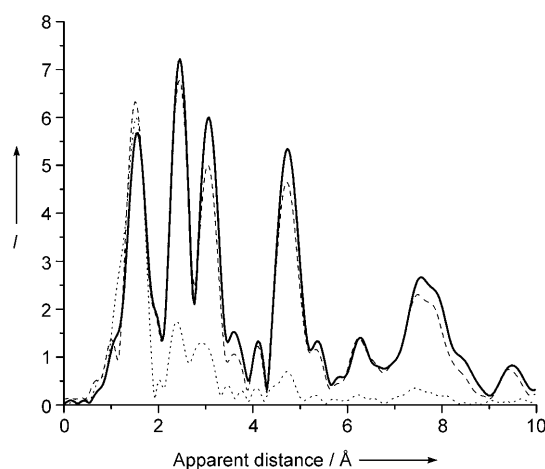

Figure 3. EXAFS spectra for bulk Co_3O_4 (——), SBA-15/Co_3O_4 (4%; -----), and SBA-15/Co_3O_4 (8%; – – –).

powder XRD results. For the 4% sample (-----), there is good agreement between the first-shell Co–O bond lengths for the nanoclusters and the bulk phase. The higher-shell Co–Co peaks, while clearly visible, have much lower intensity, indicative of very small (few nanometer) crystalline Co_3O_4 domains within the 35 nm cluster. Precedents for reduced EXAFS peak intensities arising from polycrystallinity are known.[23] We conclude that the structural characterization reveals spheroid-shaped bundles of parallel Co_3O_4 nanorods of spinel structure inside the porous SBA-15 scaffold.

Evolution of O_2 was observed by mass spectrometric monitoring of the gas in the head space of aqueous suspensions of SBA-15/Co_3O_4 catalysts driven by visible-light-generated $[Ru^{3+}(bpy)_3]$ at pH 5.8 and room temperature (476 nm, 240 mW; Figure 4 c,d). A mildly acidic pH value was
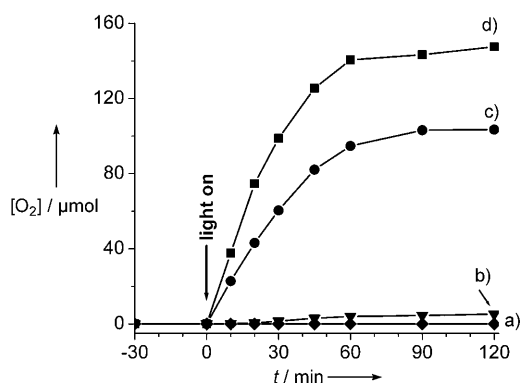

Figure 4. Oxygen evolution in aqueous suspensions (40 mL) of a) SBA-15/NiO (8%), b) micrometer-sized Co_3O_4 particles, c) SBA-15/Co_3O_4 (8%), and d) SBA-15/Co_3O_4 (4%). Measurements were conducted at pH 5.8 and 22°C. Catalysis was initiated by Ar ion laser emission at 476 nm (240 mW). Experimental details of the oxygen detection method are described in the Supporting Information.[12]

chosen to minimize photodegradation of the ruthenium complex.[24] The amount of O_2 generated increases approximately linearly for the first 30 min before gradually leveling off. When adding fresh $Na_2S_2O_8$ acceptor and readjusting the pH value to 5.8, oxygen evolution resumed at the same rate as observed initially, within uncertainties. This finding confirms that the slowdown of the water oxidation rate is principally due to the stoichiometric consumption of the persulfate acceptor and demonstrates that the activity of the Co_3O_4 nanoclusters does not degrade during photocatalysis on the time scale investigated (several hours). X-ray absorption near-edge structure (XANES) and EXAFS analysis of the Co_3O_4 clusters before and after photochemical runs did not reveal any structural or oxidation-state changes of the catalyst (see the Supporting Information).[12] NiO was prepared in SBA-15 at the same loading level (8%), and photolysis was conducted under conditions identical to those used for the SBA-15/Co_3O_4 samples.[12] As can be seen from Figure 4a, no O_2 evolution was detected, thus confirming that Co_3O_4 nanoclusters are responsible for water oxidation. We conclude that Co_3O_4 nanoclusters of spinel structure in SBA-15 silica material exhibit strong oxygen evolution activity under

mild pH and temperature conditions at an overpotential of 350 mV ($\varepsilon^o([Ru^{3+}(bpy)_3]/[Ru^{2+}(bpy)_3]) = 1.24$ V, $\varepsilon^o(O_2/H_2O) = 0.89$ V at pH 5.8).[25]

While the modest overpotential for driving the catalyst implies reasonable thermodynamic efficiency, the turnover frequency (number of oxygen molecules per second per nanocluster) and size of the catalyst determine the degree to which an integrated system featuring this catalyst will be able to keep up with the rate of incident solar photons. From the amount of O_2 gas evolved in the headspace during the first ten minutes of photolysis (Figure 4), taking into account the equilibrium oxygen concentration in the solution volume,[9] we estimate a TOF = 1140 s^{-1} per Co_3O_4 nanocluster. The calculation is based on the geometry of the bundles of Co_3O_4 nanorods described above (bundle diameter 35 nm, rod diameter 7.6 nm, typically 14 rods per bundle, average rod length 50 nm),[12] the loading of 8.4 mg, and the density of Co_3O_4 (6.07 g cm^{-3}). We conclude that values for turnover frequency and size of the Co_3O_4 nanoclusters on SBA-15 (4% loading) lie in a range adequate for quantitative use of solar photons. For the larger Co_3O_4 clusters of the SBA-15/Co_3O_4-(8%) catalyst, the estimated TOF is 3450 s^{-1}. The calculation assumes Co_3O_4 nanorod bundles of spheroid shape (average of 48 nanorods per bundle, rod diameter 7.6 nm, average rod length 130 nm).[12]

As can be seen from Figure 4, the oxygen yield is 65 times smaller for an aqueous suspension of 200 mg of bare Co_3O_4 particles of several-micrometer size (trace b) compared to that of the nanoclusters of SBA-15/Co_3O_4(4%) (containing 8.4 mg Co_3O_4) and 40 times smaller compared to the SBA-15/Co_3O_4(8%) sample (containing 17.2 mg Co_3O_4). Normalized to the same amount of Co_3O_4, the O_2 yield for the SBA-15/Co_3O_4(4%) sample exceeds that of the bare micrometer-sized particles by a factor of 1550. Clearly, the interior of the particles or clusters is not involved in the catalysis. On the other hand, assuming the geometry for the particles and nanoclusters described above and taking as nanocluster surface the combined surface area of all nanorods of the bundle (16 percent of the cobalt is at the surface), we calculate that the ratio of the total number of surface Co centers of the Co_3O_4 nanocluster sample to micrometer-sized Co_3O_4 sample is 96 in the case of SBA-15/Co_3O_4(4%). This result suggests that the much larger surface area provided by the internal nanorod structure of the Co_3O_4 clusters is a major factor for the high TOF of the nanoclusters. However, the fact that the estimate based on surface area alone falls short of the observed O_2 rate increase suggests that, in addition, Co surface sites of nanoclusters are substantially more efficient catalytically (by a factor of 16) than those of micrometer-sized particles (TOF of 0.01 s^{-1} per surface Co center for SBA-15/Co_3O_4(4%) sample compared to 0.0006 s^{-1} for micrometer-sized particles).[26] The lower O_2 product yield for SBA-15/Co_3O_4(8%) compared to SBA-15/Co_3O_4(4%) (Figure 4) despite the two times larger total number of surface Co atoms of the former may signal less efficient access of the reactant to the surface of individual nanorods in the case of the larger nanorod bundles.

The quantum efficiency of the $[Ru^{2+}(bpy)_3]$/persulfate system used herein for driving the water oxidation catalyst is

Communications

calculated as 18% for the SBA-15/Co$_3$O$_4$(4%) experiment (two times the number of O$_2$ molecules produced divided by the number of photons absorbed by the sensitizer).[4] This quantum yield is only a lower limit, because it is assumed that all photons are absorbed by the sensitizer in the strongly scattering suspension, which is an overestimation. The value is influenced by several factors, including the efficiency of electron transfer between the excited [Ru^{2+}(bpy)$_3$] sensitizer and the S$_2$O$_8^{2-}$ acceptor and the efficiency of charge transfer between Co$_3$O$_4$ nanoclusters and [Ru^{3+}(bpy)$_3$] inside the silica mesopores. Hence, the quantum yield may depend on the particular sensitizer used for driving the catalyst. Note that the turnover frequencies were not limited by the visible light intensity and are therefore intrinsic properties of the Co$_3$O$_4$ catalysts.

In conclusion, oxygen evolution at nanostructured Co$_3$O$_4$ clusters in mesoporous silica reported herein constitutes the first observation of efficient water oxidation by a nanometer-sized multielectron catalyst made of a first-row transition-metal oxide. We have previously shown that metal oxide nanocluster catalysts for water oxidation can be driven efficiently by visible-light-absorbing binuclear charge-transfer chromophores,[9] which are of few ångström size. Therefore, rates and size of the catalyst including chromophore are comparable to nature's photosystem II, in which the majority of the space is taken up by the light-harvesting system rather than the catalyst. The abundance of the metal oxide, the stability of the nanoclusters under use, the modest over-potential, and the mild pH and temperature conditions make this a promising catalytic component for developing a viable integrated solar fuel conversion system, the next important challenge in this field.

Experimental Section

The synthesis of the catalysts is described in detail in the Supporting Information.

The materials were characterized by transmission electron microscopy (TEM, LIBRA at NCEM), powder X-ray diffraction (PXRD, Siemens model D500 diffractometer equipped with Cu$_{K\alpha1}$ radiation, $\lambda = 1.541$ Å), and N$_2$ adsorption (Quantachrome Autosorb 1). XANES and EXAFS data were collected at Beam line 7.3 of SSRL. The data were treated by the Ifeffit software. The photolysis experiments were conducted with a continuous visible laser source and mass spectrometric monitoring of oxygen, as described in the Supporting Information.

[1] http://rredc.nrel.gov/solar/spectra/am1.5.
[2] J. Kiwi, M. Grätzel, *Angew. Chem.* **1978**, *90*, 900; *Angew. Chem. Int. Ed. Engl.* **1978**, *17*, 860.
[3] J. M. Lehn, J. P. Sauvage, R. Ziessel, *Nouv. J. Chim.* **1980**, *4*, 355.
[4] A. Harriman, I. J. Pickering, J. M. Thomas, P. A. Christensen, *J. Chem. Soc. Faraday Trans. 1* **1988**, *84*, 2795.
[5] M. Hara, J. T. Lean, T. E. Mallouk, *Chem. Mater.* **2001**, *13*, 4668.
[6] N. D. Morris, M. Suzuki, T. E. Mallouk, *J. Phys. Chem. A* **2004**, *108*, 9115.
[7] P. G. Hoertz, Y. I. Kim, W. J. Youngblood, T. E. Mallouk, *J. Phys. Chem. B* **2007**, *111*, 6845.
[8] M. Yagi, E. Tomita, S. Sakita, T. Kuwabara, K. Nagai, *J. Phys. Chem. B* **2005**, *109*, 21489.
[9] H. Han, H. Frei, *J. Phys. Chem. C* **2008**, *112*, 16156.
[10] R. Nakamura, H. Frei, *J. Am. Chem. Soc.* **2006**, *128*, 10668.
[11] J. Yano, J. Kern, K. Sauer, M. J. Latimer, Y. Pushkar, J. Biesiadka, B. Loll, W. Saenger, J. Messinger, A. Zouni, V. K. Yachandra, *Science* **2006**, *314*, 821.
[12] See the Supporting Information.
[13] T. Schmidt, H. Wendt, *Electrochim. Acta* **1994**, *39*, 1763.
[14] C. Iwakura, A. Honji, H. Tamura, *Electrochim. Acta* **1981**, *26*, 1319.
[15] P. Rasiyah, A. C. C. Tseung, *J. Electrochem. Soc.* **1983**, *130*, 365.
[16] R. N. Singh, D. Mishra, Anindita, A. S. K. Sinha, A. Singh, *Electrochem. Commun.* **2007**, *9*, 1369.
[17] M. W. Kanan, D. G. Nocera, *Science* **2008**, *321*, 1072.
[18] M. Morita, C. Iwakura, H. Tamura, *Electrochim. Acta* **1977**, *22*, 325.
[19] A. Kay, I. Cesar, M. Grätzel, *J. Am. Chem. Soc.* **2006**, *128*, 15714.
[20] D. Y. Zhao, J. L. Feng, Q. S. Huo, N. Melosh, G. H. Fredrickson, B. F. Chmelka, G. D. Stucky, *Science* **1998**, *279*, 548.
[21] F. Jiao, K. M. Shaju, P. G. Bruce, *Angew. Chem.* **2005**, *117*, 6708; *Angew. Chem. Int. Ed.* **2005**, *44*, 6550.
[22] B. Z. Tian, X. Y. Liu, H. F. Yang, S. H. Xie, C. Z. Yu, B. Tu, D. Y. Zhao, *Adv. Mater.* **2003**, *15*, 1370.
[23] K. Maeda, K. Teramura, D. L. Lu, N. Saito, Y. Inoue, K. Domen, *J. Phys. Chem. C* **2007**, *111*, 7554.
[24] M. Hara, C. C. Waraksa, J. T. Lean, B. A. Lewis, T. E. Mallouk, *J. Phys. Chem. A* **2000**, *104*, 5275.
[25] *CRC Handbook of Chemistry and Physics*, 85th ed. (Ed.: D. R. Lide), CRC, Boca Raton, FL, **2004**, pp. 8–27.
[26] While we observed a very small amount of oxygen evolution for micrometer-sized Co$_3$O$_4$ particles upon photolysis using experimental procedures identical to those described in the literature (Ref. [4]), we did not observe the much higher water oxidation rates reported by the previous authors.